Anisotropic physical properties of the Taylor-phase T-Al72.5Mn21.5Fe6.0 complex intermetallic

Heggen, M.; Feuerbacher, M.; Ivkov, Jovica; Popčević, Petar; Batistić, Ivo; Smontara, Ana; Jagodič, Marko; Jagličić, Zvonko; Janovec, J.; Wencka, M.; ...

Source / Izvornik: **Physical review B: Condensed matter and materials physics, 2010, 81**

Journal article, Published version
Rad u časopisu, Objavljena verzija rada (izdavačev PDF)

https://doi.org/10.1103/PhysRevB.81.184204

Permanent link / Trajna poveznica: https://urn.nsk.hr/urn:nbn:hr:217:789375

Anisotropic physical properties of the Taylor-phase T-$Al_{72.5}Mn_{21.5}Fe_{6.0}$ complex intermetallic

M. Heggen,[1] M. Feuerbacher,[1] J. Ivkov,[2] P. Popčević,[2] I. Batistić,[3] A. Smontara,[2] M. Jagodič,[4] Z. Jagličić,[4] J. Janovec,[5] M. Wencka,[6,*] and J. Dolinšek[6]

[1]*Institut für Festkörperforschung, Forschungszentrum Jülich, Jülich D-52425, Germany*

[2]*Institute of Physics, Laboratory for the Physics of Transport Phenomena, Bijenička 46, P.O. Box 304, HR-10001 Zagreb, Croatia*

[3]*Department of Physics, University of Zagreb, Bijenička 32, P.O. Box 331, HR-10002 Zagreb, Croatia*

[4]*Institute of Mathematics, Physics and Mechanics, University of Ljubljana, Jadranska 19, SI-1000 Ljubljana, Slovenia*

[5]*Faculty of Materials Science and Technology, Slovak University of Technology, J. Bottu 25, 917 24 Trnava, Slovak Republic*

[6]*J. Stefan Institute, University of Ljubljana, Jamova 39, SI-1000 Ljubljana, Slovenia*

(Received 4 March 2010; published 7 May 2010)

We have investigated anisotropic physical properties (the magnetic susceptibility, the electrical resistivity, the thermoelectric power, the Hall coefficient and the thermal conductivity) of the single-crystalline Taylor-phase T-$Al_{72.5}Mn_{21.5}Fe_{6.0}$ complex intermetallic that is an orthorhombic approximant to the *d*-Al-Mn-Pd decagonal quasicrystal. The measurements were performed along the *a*, *b*, and *c* directions of the orthorhombic unit cell, where (a,c) atomic planes are stacked along the perpendicular *b* direction. The T-$Al_{72.5}Mn_{21.5}Fe_{6.0}$ shows spin-glass behavior below the spin-freezing temperature $T_f \approx 29$ K with a small anisotropy in the magnetic susceptibility. The anisotropic electrical resistivities are rather large and show negative temperature coefficient. The resistivity is lowest along the stacking direction, which appears to be a common property of the decagonal-approximant phases with a stacked-layer structure. The temperature-dependent resistivity was theoretically reproduced by the quantum transport theory of slow charge carriers. The thermopower is positive for all three crystallographic directions, indicating that holes are the majority charge carriers, and no anisotropy can be claimed within the experimental precision. The same conclusion on the holes being the dominant charge carriers follows from the Hall-coefficient measurements, which is a sum of the (positive) normal Hall coefficient and the anomalous term, originating from the magnetization. The anisotropy of the thermal conductivity is practically negligible. The T-$Al_{72.5}Mn_{21.5}Fe_{6.0}$ Taylor phase can be considered as a "close-to-isotropic" complex intermetallic. The relation of the anisotropic physical properties of the Taylor phase to other families of decagonal-approximant phases with the stacked-layer structure is discussed.

DOI: 10.1103/PhysRevB.81.184204 PACS number(s): 61.44.Br, 71.23.Ft

I. INTRODUCTION

Decagonal quasicrystals (*d*-QCs) can be structurally viewed as a periodic stack of quasiperiodic atomic planes, so that *d*-QCs are two-dimensional (2D) quasicrystals, whereas they are periodic crystals in a direction perpendicular to the quasiperiodic planes. A consequence of the structural anisotropy are anisotropic magnetic, electrical, and thermal transport properties, when measured along the periodic and quasiperiodic crystallographic directions. The lack of translational periodicity within the quasiperiodic planes prevents any quantitative theoretical analysis of the anisotropic physical properties of *d*-QCs. The problem can be overcome by considering approximant phases to the decagonal phase, for which—being periodic solids in three dimensions (3D)—theoretical simulations are straightforward to perform. Approximant phases are characterized by large unit cells, which periodically repeat in space with the atomic decoration closely resembling that of the *d*-QCs. Atomic layers are again stacked periodically and the periodicity lengths along the stacking direction are almost identical to those along the periodic direction of *d*-QCs. Moreover, atomic planes of approximants and *d*-QCs show locally similar patterns, so that their structures on the scale of near-neighbor atoms closely resemble each other. Decagonal approximants thus offer valid comparison to the *d*-QCs.

The degree of anisotropy of the physical properties of *d*-QCs is related to the structural details of a particular decagonal phase, depending on the number of quasiperiodic layers in one periodic unit.[1,2] The most anisotropic case are the phases with just two layers, realized in *d*-Al-Ni-Co and *d*-Al-Cu-Co, where the periodicity length along the periodic axis is about 0.4 nm. Other *d* phases contain more quasiperiodic layers in a periodic unit and show smaller anisotropies. In *d*-Al-Co, *d*-Al-Ni, and *d*-Al-Si-Cu-Co there are four quasiperiodic layers with the periodicity about 0.8 nm; *d*-Al-Mn, *d*-Al-Cr, and *d*-Al-Mn-Pd phases contain six layers with the periodicity of about 1.2 nm, whereas *d*-Al-Pd and *d*-Al-Cu-Fe phases contain eight layers in a periodicity length of 1.6 nm. Recently, large single-crystalline samples of several decagonal-approximant phases were successfully grown and their anisotropic physical properties (the magnetic susceptibility, the electrical resistivity, the thermoelectric power, the Hall coefficient and the thermal conductivity) were measured along three orthogonal crystallographic directions. The first was the $Al_{76}Co_{22}Ni_2$ compound,[3,4] known as the Y-phase of Al-Ni-Co (denoted as Y-Al-Ni-Co), which belongs to the $Al_{13}TM_4$ (TM=transition metal) class of complex intermetallics and is a monoclinic approximant to the decagonal phase with two atomic layers within one periodic unit of ≈ 0.4 nm along the stacking direction and a relatively small unit cell, comprising 32 atoms. The second group were the orthorhombic o-$Al_{13}Co_4$ (Ref. 5), the monoclinic $Al_{13}Fe_4$ and its ternary extension $Al_{13}(Fe,Ni)_4$ (Ref. 6) decagonal approximants, also belonging to the $Al_{13}TM_4$ class of intermetallics, but comprising four atomic layers

within one periodic unit of ≈0.8 nm along the stacking direction and a larger unit cell containing 102 atoms. The third was the $Al_4(Cr,Fe)$ compound with composition $Al_{80}Cr_{15}Fe_5$,[7,8] belonging to the class of orthorhombic Al_4TM phases first described by Deng *et al.*,[9] which are approximants to the decagonal phase with six atomic layers in a periodic unit of 1.25 nm and 306 atoms in the giant unit cell. Common to all these phases are strongly anisotropic magnetic, electrical, and thermal transport properties between the stacking and the in-plane directions, where the crystals show the highest conductivity for both the electricity and heat along the stacking direction (corresponding to the periodic tenfold direction in *d*-QCs), whereas the in-plane anisotropy is considerably smaller, yet significant. For the Y-Al-Ni-Co and o-$Al_{13}Co_4$ phases, the origin of the anisotropy was analyzed in terms of the *ab initio* calculated anisotropic Fermi surface, using published structural models.

In this paper we present anisotropic physical properties of the orthorhombic Taylor phase T-Al-Mn-Fe of composition $Al_{72.5}Mn_{21.5}Fe_{6.0}$ that is an approximant to the *d*-Al-Mn-Pd quasicrystal with six atomic layers within one periodic unit of ≈1.2 nm and 156 atoms in the unit cell. We show that although the T-Al-Mn-Fe phase is another decagonal-approximant phase, its physical properties are quite different from those of the above-mentioned decagonal-approximant phases from the $Al_{13}TM_4$ and Al_4TM families, so that no common behavior of the decagonal-approximant phases can be claimed.

II. STRUCTURAL CONSIDERATIONS AND SAMPLE PREPARATION

The binary Taylor-phase T-Al_3Mn orthorhombic approximant to the decagonal phase and its ternary extensions T-$Al_3(Mn,Pd)$ and T-$Al_3(Mn,Fe)$ are all structurally isomorphic. The structure of the binary T-Al_3Mn was first solved by Hiraga *et al.*,[10] whereas the model of T-$Al_3(Mn,Pd)$ with composition $Al_{72.3}Mn_{24.5}Pd_{3.2}$ was reported by Klein *et al.*[11] Within the Klein model,[11] the T-$Al_3(Mn,Pd)$ phase is described as an independent ternary phase structurally similar to binary T-Al_3Mn, whereas Balanetskyy *et al.*[12] have reported that this phase is not an independent ternary phase, but a ternary solid solution of Pd in the binary T-Al_3Mn. The same consideration holds for the ternary solid solution T-$Al_3(Mn,Fe)$. The structure of the Taylor phase is built of two atomic layers within the (a,c) planes stacked along the *b* pseudotenfold crystallographic axis, a flat layer F and a puckered layer composed of two sublayers P1 and P2. The layers are located at $y \approx 0.25$, 0.38, and 0.43 and there are six layers within one periodic unit. The orthorhombic unit cell (space group *Pnma*) contains 156 atoms and the lattice parameters of the binary T-phase are[13] $a=1.48$ nm, $b=1.24$ nm and $c=1.26$ nm [the values for the T-$Al_3(Mn,Pd)$ and T-$Al_3(Mn,Fe)$ solid solutions are very similar]. Most of the lattice sites show either fractional occupation (the sites are too close in space to be occupied simultaneously) or mixed TM/Al occupancy, so that there exists structural and chemical disorder on the lattice. Majority of the atoms are clustered in the form of pentagonal prisms and antiprisms.

The T-phase in the Al-Mn-Fe system is stable at high temperatures only, similar to the T-phase in the binary Al-Mn system. It is observed at room temperature (RT) only due to rapid quenching of the material after the growth. On the other hand, the T-phase in the Al-Mn-Pd system remains stable also at lower temperatures. From this point of view, the T-phase in the Al-Mn-Fe system is more similar to the binary T-phase in the Al-Mn system than to the ternary one in the Al-Mn-Pd system. The reason is probably the fact that the similarity between the manganese and iron atoms is higher than the similarity between the manganese and palladium atoms; iron is just beside manganese in the periodic table. It was also reported that the $Al_{73}Mn_{21}Fe_6$ composition behaves special as additional annealing of the quenched T-$Al_{73}Mn_{21}Fe_6$ Taylor phase resulted in a transformation to the decagonal phase.[14]

Our study of the anisotropic physical properties of the Taylor phase was performed on an oriented single crystal T-$Al_{72.5}Mn_{21.5}Fe_{6.0}$ grown by the Czochralski technique. The crystal was pulled from a melt of composition $Al_{75}Mn_{20}Fe_5$ at a rate 1 mm/h under Argon atmosphere. The growth was performed in a temperature range between 1100 and 1040 °C according to the phase-diagram information and growth conditions reported by Balanetskyy and co-workers.[12] The material was not annealed after growth. In order to perform crystallographic-direction-dependent studies, three rectangular bar-shaped samples of dimensions $2 \times 1 \times 1$ mm^3 were cut from the oriented single crystal with their long axes along the *a*, *b*, and *c* crystallographic directions, where for each sample, the orientation of the other two axes was known as well. The so-prepared samples enabled us to determine the anisotropic physical properties of the T-$Al_3(Mn,Fe)$ Taylor phase along the three orthogonal directions.

Recently we have reported[15] the magnetic properties of a polygrain binary T-Al_3Mn and a ternary T-$Al_3(Mn,Pd)$ and T-$Al_3(Mn,Fe)$ series of samples of compositions T-$Al_{73}Mn_{27-x}Pd_x$ $(x=2,4,6)$ and T-$Al_{73}Mn_{27-x}Fe_x$ $(x=2,4)$ and the decagonal quasicrystal *d*-$Al_{73}Mn_{21}Fe_6$. All samples exhibited a pronounced magnetic memory effect that has lead to the application of this material for the thermal storage of digital information, serving as a new kind of a digital memory element—a thermal memory cell,[16] where the digital information is stored into the bulk of the material by pure thermal manipulation, in the absence of any electric, magnetic, or electromagnetic field. The electrical resistivity and the Hall coefficient of the polygrain T-Al_3Mn, T-$Al_{73}Mn_{27-x}Fe_x$ $(x=2,4)$ and the decagonal quasicrystal *d*-$Al_{73}Mn_{21}Fe_6$ were reported as well.[17]

We also mention that the single crystal of composition $Al_{72.5}Mn_{21.5}Fe_{6.0}$ pertinent to this study was a Taylor phase, whereas the polycrystalline material of almost identical composition $Al_{73}Mn_{21}Fe_6$ reported in the preceding papers[15,17] was a decagonal quasicrystal. As discussed above, different annealing conditions may be the reason for this discrepancy.

III. ANISOTROPIC PHYSICAL PROPERTIES OF THE SINGLE-CRYSTALLINE T-$Al_{72.5}Mn_{21.5}Fe_{6.0}$

A. Magnetization and magnetic susceptibility

Magnetic properties of the polygrain binary T-Al_3Mn and the ternary T-$Al_{73}Mn_{27-x}Pd_x$ $(x=2,4,6)$, T-$Al_{73}Mn_{27-x}Fe_x$

($x=2,4$) and the decagonal quasicrystal d-$Al_{73}Mn_{21}Fe_6$ were reported recently in a comprehensive study.[15] The results can be summarized as follows. (1) All samples show a transition to a spin-glass-type nonergodic phase at the spin-freezing temperature $T_f \approx 20-23$ K, where below T_f, the zero-field-cooled (zfc) and field-cooled (fc) magnetic susceptibilities become unequal. This shows frustration of interactions between the magnetic moments of the Mn and Fe ions. (2) Within the nonergodic phase, typical broken-ergodicity phenomena were observed, including the frequency-dependent freezing temperature, $T_f(\omega)$, hysteresis and remanence, ultraslow decay of the thermoremanent magnetization, the memory effect (a state of the spin system reached upon isothermal aging can be retrieved after a negative temperature cycle) and rejuvenation (small positive temperature cycle within the nonergodic phase erases the effect of previous aging). (3) The memory effect was employed to construct a new kind of a memory element using the T-Al_3(Mn,Fe) material, where an eight-bit byte of digital information was stored by a specific temperature-time profile in the absence of any external electric, magnetic, or electromagnetic field.[16] In this way, arbitrary ASCII characters, representing text in computers, were successfully written by pure thermal manipulation of the Taylor-phase polygrain material. Our single-crystalline T-$Al_{72.5}Mn_{21.5}Fe_{6.0}$ sample was subjected to the same set of magnetic experiments as the polygrain material studied in Ref. 15, and the results are in complete accordance with those of the polygrain samples. Since the polygrain and single-crystalline morphologies mainly affect the long-range electrical and thermal transport properties of the material, where the electrons and phonons travel over macroscopic distances, no pronounced differences between the magnetic properties of the polygrain and the single-crystalline samples are expected. We, therefore, do not repeat here the general magnetic results of the Taylor phase, but rather concentrate on the anisotropy of magnetic properties of the single-crystalline T-$Al_{72.5}Mn_{21.5}Fe_{6.0}$.

Magnetic properties were investigated in the temperature interval between 300 and 2 K and magnetic fields up to 50 kOe using a Quantum Design MPMS XL-5 SQUID magnetometer. In the orientation-dependent measurements, the magnetic field was directed along the long axis of each sample, thus along the a, b, and c crystallographic directions.

1. zfc and fc magnetic susceptibilities

The zfc and fc susceptibilities $\chi = M/H$ in the temperature range 2–50 K in magnetic fields $H=100$ Oe and 50 kOe are shown in Fig. 1. In the following, the anisotropic susceptibilities are labeled by the index k, denoting the direction of the magnetic field with respect to the crystallographic axes ($k=a,b,c$). In the low field of 100 Oe [Fig. 1(a)], χ^k_{zfc}'s exhibit a pronounced cusp at the spin-freezing temperature $T_f=29$ K, whereas χ^k_{fc}'s remain more or less constant below T_f. At T_f, the system becomes nonergodic and χ^k_{zfc} and χ^k_{fc} become unequal. The orientation-dependent susceptibilities show the following anisotropy: there is practically no anisotropy between the two in-plane directions a and c, whereas there exists a moderate anisotropy between the in-plane and the stacking b directions, where the susceptibility along b is somewhat higher. The temperature-dependent susceptibility difference $\chi^k_{\mathrm{fc}} - \chi^k_{\mathrm{zfc}}$ below T_f does not show anisotropy and there is also no anisotropy in the freezing temperature for the three crystallographic directions. The lack of anisotropy in T_f was verified also from the orientation-dependent measurements of the ac susceptibility χ' (not shown), where the temperature of the cusp in χ' did not depend on the direction of the magnetic field. It is worth mentioning that $T_f=29$ K of the single-crystalline T-$Al_{72.5}Mn_{21.5}Fe_{6.0}$ is by $\Delta T=7$ K higher from that of the polygrain decagonal quasicrystal d-$Al_{73}Mn_{21}Fe_6$ ($T_f=22$ K) of practically the same composition, studied in the preceding paper.[15] Different structures of the two compounds, the small difference in the transition-metal (Mn+Fe) concentration and the extrinsic disorder effects in the polygrain sample may be at the origin of this difference.

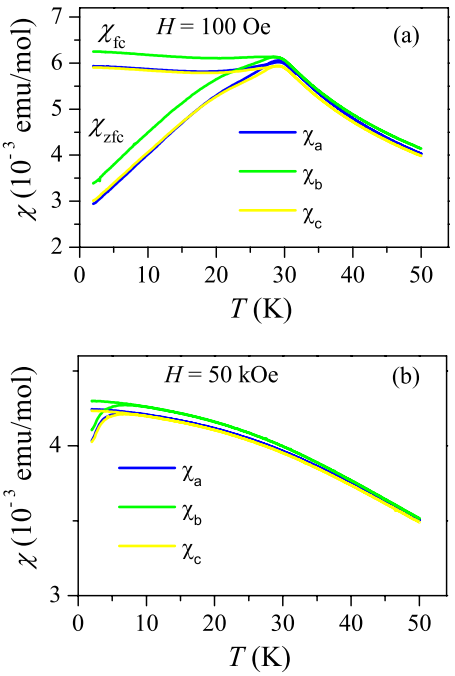

FIG. 1. (Color online) Anisotropic field-cooled (fc) and zero-field-cooled (zfc) magnetic susceptibilities of the single-crystalline T-$Al_{72.5}Mn_{21.5}Fe_{6.0}$ in the temperature range 2–50 K and magnetic field (a) 100 Oe and (b) 50 kOe, directed along the a, b, and c crystallographic directions. The susceptibilities are calculated per mol of $Al_{0.725}Mn_{0.215}Fe_{0.06}$ "molecules" with the molar mass 34.724 g/mol.

The χ^k_{zfc} and χ^k_{fc} in the high field of 50 kOe are displayed in Fig. 1(b). We observe that the cusp in χ^k_{zfc} has rounded and the zfc-fc splitting temperature has shifted to lower temperature of about 8 K. This strong influence of the external magnetic field demonstrates comparable strengths of the spin-spin exchange interactions (responsible for the spin-glass magnetic ordering in the absence of an external magnetic field) and the Zeeman interaction of spins with the magnetic field. The internal spin-glass-type frustrated magnetic structure is thus "soft" and fragile with respect to the external magnetic field. The anisotropy of the susceptibility is preserved in the high field [Fig. 1(b)]. There is again no anisotropy between the two in-plane directions a and c and a

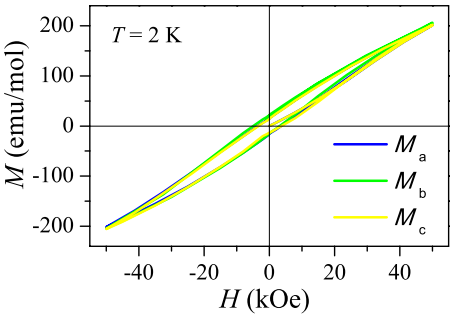

FIG. 2. (Color online) The $M(H)$ hysteresis loops at $T=2$ K for the field along the three crystallographic directions a, b, and c in the sweep range ± 50 kOe. The three loops are practically indistinguishable on the graph.

moderate anisotropy to the stacking b direction. The susceptibility difference $\chi^k_{\rm fc}-\chi^k_{\rm zfc}$ does not show anisotropy either.

2. Hysteresis

The $M(H)$ curves for the field along the three crystallographic directions a, b, and c in the sweep range ± 50 kOe and temperature $T=2$ K are displayed in Fig. 2. The magnetization curves show hysteresis, but there is no anisotropy between the three directions, in agreement with the previous result that the susceptibility difference $\chi^k_{\rm fc}-\chi^k_{\rm zfc}$ does not show anisotropy [recall that the difference between the fc and zfc magnetizations, $M^k_{\rm fc}-M^k_{\rm zfc}$, represents the remanent magnetization that is the source of the $M(H)$ hysteresis]. The $M(H)$ loops remain open up to the highest applied field of 50 kOe, demonstrating predominant antiparallel (antiferromagnetic) coupling between the spins (for the parallel ferromagnetic-type coupling, the loops usually saturate at a much lover field of a few kOe only).

3. Memory effect

The memory effect (ME) is the most spectacular manifestation of the out-of-equilibrium dynamics of a nonergodic magnetically frustrated spin system, where a state of the spin system reached at a given temperature upon isothermal aging for a time t_w can be retrieved after a negative temperature cycle. In the ME experiment, the spin system is cooled continuously from the paraphase below the freezing temperature T_f in zero magnetic field and the cooling is stopped at the aging temperature $T_1<T_f$ for a time t_w of the order of minutes to hours. The cooling then resumes to the lowest temperature where a small magnetic field is applied and the zfc magnetization $M_{\rm zfc}$ is measured in a continuous heating run. The memory is imprinted in $M_{\rm zfc}$, which shows a dip at the aging temperature T_1. The memory imprint is best presented by showing the difference between the reference $M_{\rm zfc}$ curve of a continuous $(t_w=0)$ cooling run and the curve with aging at T_1 for a time t_w, $\Delta M=M_{\rm zfc}(t_w=0)-M_{\rm zfc}(t_w)$, where ΔM appears in the form of a resonant peak at the aging temperature T_1. Further details of the ME experiments in the Taylor-phase material are given in the previous paper.[15] Here we concentrate on the possible anisotropy of the ME for the field along different crystallographic directions.

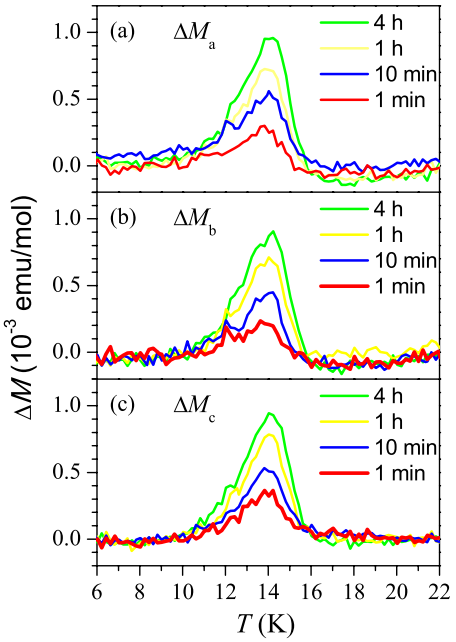

FIG. 3. (Color online) Anisotropy of the memory effect in the single-crystalline T-$Al_{72.5}Mn_{21.5}Fe_{6.0}$, by showing the difference $\Delta M=M_{\rm zfc}(t_w=0)-M_{\rm zfc}(t_w)$ between the reference (no-stop) zfc magnetization curve $M_{\rm zfc}(t_w=0)$ and the zfc magnetization curves $M_{\rm zfc}(t_w)$ with a stop at the aging temperature $T_1=14$ K for aging times t_w between 1 min and 4 h. For more details on the memory effect see Ref. 15. In the panels (a), (b), and (c), the magnetic field was directed along the a, b, and c crystallographic directions, respectively.

Our ME experiments on the single-crystalline T-$Al_{72.5}Mn_{21.5}Fe_{6.0}$ ($T_f=29$ K) were performed at a set of different aging temperatures T_1 between T_f and 4 K and aging times between 1 min and 4 h. No anisotropy of the ME between the three crystallographic directions was observed. This is evident from Fig. 3, where we show ΔM_k for a representative aging temperature $T_1=14$ K and a set of aging times. The $\Delta M_k(t_w)$ curves for the $k=a$, b, and c directions of the magnetic field are indistinguishable within the experimental error of measurement. Using the Taylor-phase material for the thermal memory cell application[16] is thus advantageous, as identical thermal-storage performance is obtained for the single crystalline and polygrain forms of the material, where the latter is much easier to synthesize.

4. Paramagnetic susceptibility

We discuss also the paramagnetic susceptibility, which will be employed for the analysis of the temperature-dependent Hall coefficient, to be presented in the following. The zfc and fc susceptibilities, $\chi^k_{\rm zfc}$ and $\chi^k_{\rm fc}$, in the temperature range 2–300 K, measured in a magnetic field $H=1$ kOe along the three crystallographic directions a, b, and c are displayed in Fig. 4(a). The experimental anisotropy of the paramagnetic susceptibility is rather small, less than 2%, and cannot be discerned from the graph. The temperature-dependent paramagnetic susceptibility in the high-temperature range $T>60$ K was analyzed with the Curie-Weiss function

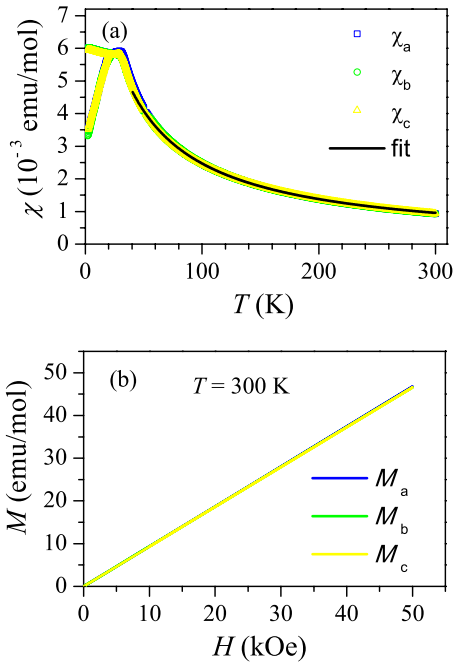

FIG. 4. (Color online) (a) The anisotropic zfc and fc susceptibilities in the temperature range 2–300 K, measured in a magnetic field $H=1$ kOe along the three crystallographic directions a, b, and c. Solid curve is the Curie-Weiss fit with Eq. (1) in the high-temperature $T>60$ K paramagnetic regime and the fit parameters are given in the text. For $T>60$ K, the three sets of experimental data and the fitting curve are indistinguishable, so that the same fit is valid for all three directions. (b) The $M(H)$ lines at $T=300$ K in the paramagnetic phase for the field along the three crystallographic directions. The three lines are indistinguishable on the graph.

$$\chi = \chi_0 + \frac{C}{T-\theta}, \tag{1}$$

where χ_0 is the temperature-independent part (including the Larmor diamagnetic core susceptibility χ_{dia} and the Pauli paramagnetic and Landau diamagnetic susceptibilities of conduction electrons), C is the Curie-Weiss constant and θ the Curie-Weiss temperature. Due to the very small anisotropy of the paramagnetic susceptibility, only one set of fit parameters (χ_0, C, and θ) was determined that should be considered valid for all three directions. The fit [solid curve in Fig. 4(a)] yielded the parameter values $\chi_0=-4\times10^{-6}$ emu/mol, $C=0.31$ emu K/mol, and $\theta=-27$ K. The negative θ value supports the consideration of a predominant antiferromagnetic coupling between the magnetic moments. The Larmor contribution was estimated theoretically from literature tables[18] to be in the range $\chi_{dia}=[-3.8,-5.2]\times10^{-6}$ emu/mol (depending on the Mn and Fe ionization states), which is about the same as χ_0.

The $M(H)$ curves at $T=300$ K in the paramagnetic phase for the field along the three crystallographic directions are shown in Fig. 4(b). The curves do not show any anisotropy and hysteresis, but a linear $M(H)$ relation typical of Curie-type paramagnets.

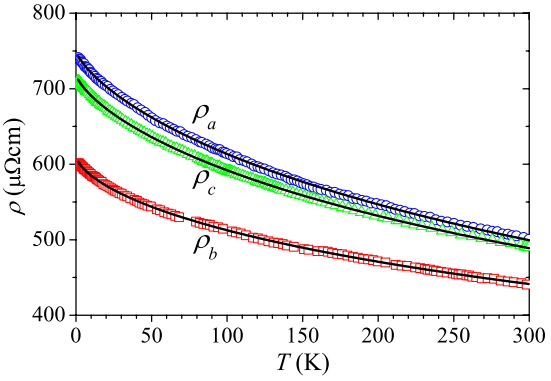

FIG. 5. (Color online) Temperature-dependent electrical resistivity of T-$Al_{72.5}Mn_{21.5}Fe_{6.0}$ along the three orthogonal crystallographic directions a, b, and c. Solid curves represent the fits with Eq. (3) using the quantum transport theory of slow charge carriers, and the fit parameters are collected in Table I.

B. Electrical resistivity

The electrical resistivity of the single-crystalline T-$Al_{72.5}Mn_{21.5}Fe_{6.0}$ was measured between 300 and 2 K using the standard four-terminal technique. The $\rho(T)$ data for the current along the three crystallographic directions are displayed in Fig. 5. All resistivities show a negative temperature coefficient (NTC) by increasing with decreasing temperature. The resistivity is the lowest along the stacking b direction perpendicular to the atomic planes, where its RT value amounts $\rho_b^{300\ \mathrm{K}}=441\ \mu\Omega$ cm and the 2 K resistivity is $\rho_b^{2\ \mathrm{K}}=601\ \mu\Omega$ cm, yielding the increase upon cooling by $(\rho_b^{2\ \mathrm{K}}-\rho_b^{300\ \mathrm{K}})/\rho_b^{300\ \mathrm{K}}=40\%$. The two in-plane resistivities ρ_a and ρ_c are higher, amounting $\rho_a^{300\ \mathrm{K}}=501\ \mu\Omega$ cm and $\rho_a^{2\ \mathrm{K}}=740\ \mu\Omega$ cm with the increase $(\rho_a^{2\ \mathrm{K}}-\rho_a^{300\ \mathrm{K}})/\rho_a^{300\ \mathrm{K}}=48\%$, whereas $\rho_c^{300\ \mathrm{K}}=490\ \mu\Omega$ cm and $\rho_c^{2\ \mathrm{K}}=709\ \mu\Omega$ cm with $(\rho_c^{2\ \mathrm{K}}-\rho_c^{300\ \mathrm{K}})/\rho_c^{300\ \mathrm{K}}=45\%$. Considering the experimental error to be about 5% (originating mainly from the uncertainty in the samples' geometrical parameters), no pronounced anisotropy between the two in-plane a and c directions can be claimed, whereas the anisotropy to the stacking b direction is significant, though still small (at 300 K, the ρ_b value is 10% smaller from ρ_a and ρ_c). It is remarkable that this kind of anisotropy, where the resistivity is lowest along the stacking direction, whereas the in-plane resistivities are higher and show little or no anisotropy, appears to be a general feature of the decagonal-approximant phases with the stacked-layer structure. It was equally observed in the Y-Al-Ni-Co (Refs. 3 and 4), the o-$Al_{13}Co_4$ (Ref. 5), the $Al_{13}Fe_4$ and $Al_{13}(Fe,Ni)_4$ (Ref. 6) and the $Al_4(Cr,Fe)$ (Refs. 7 and 8) decagonal approximants. It is also noteworthy that the anisotropic resistivity values of the investigated single-crystalline T-$Al_{72.5}Mn_{21.5}Fe_{6.0}$ from Fig. 5 are by factors 2–10 smaller from the resistivities of the polygrain T-Al_3Mn, T-$Al_{73}Mn_{27-x}Fe_x$ ($x=2,4$) and the decagonal quasicrystal d-$Al_{73}Mn_{21}Fe_6$ reported in the previous paper.[17] Though different chemical compositions of the samples (and the structural difference in the case of the decagonal d-$Al_{73}Mn_{21}Fe_6$) are likely the dominant cause of these differences, the extrinsic effects due to the polygrain morphology of the samples (grain boundaries) may add significantly to the higher resistivity of the polygrain samples.

A straightforward way to analyze theoretically the anisotropic resistivity of the T-$Al_{72.5}Mn_{21.5}Fe_{6.0}$ single crystal is to calculate *ab initio* the anisotropic Fermi surface using published structural models of the T-phase and then perform calculation of the electronic transport coefficients (the electrical resistivity, the thermoelectric power, the Hall coefficient and the electronic contribution to the thermal conductivity) using appropriate transport theory, e.g., the semiclassical Bloch-Boltzmann theory. Such calculations were successfully performed for the Y-Al-Ni-Co (Refs. 3 and 4) and $Al_{13}Co_4$ (Ref. 5) decagonal approximants. In the case of the T-Al_3(Mn,Fe) phase, there are three major problems to perform such calculations. First, to calculate *ab initio* the Fermi surface, one has to have a reliable structural model of the T-phase for the particular composition $Al_{72.5}Mn_{21.5}Fe_{6.0}$ of our sample, which is not available at present. Second, in the unit cells of the related T-phase models, e.g., the model with composition $Al_{72.3}Mn_{24.5}Pd_{3.2}$ by Klein *et al.*,[11] most of the lattice sites show either fractional occupation or mixed TM/Al occupancy, creating structural and chemical disorder on the lattice. For the *ab initio* calculations, the unit cell should be well defined by having a particular fractionally occupied lattice site either occupied with an atom (occupation 1) or the site is empty (occupation 0) and the sites of mixed occupancy should either contain an Al or a TM atom. Since out of the 25 atomic sites in the unit cell of the Klein *et al.*[11] model, 11 are fractionally occupied and 6 show mixed occupancy, many different variants of the unit cell can be constructed and most of them will give different results. Third, the NTC resistivity cannot be reproduced within the Bloch-Boltzmann transport theory, which is thus inapplicable to our T-$Al_{72.5}Mn_{21.5}Fe_{6.0}$ single crystal. In this situation, we proceed with the resistivity analysis in a semiquantitative way by employing the theory of quantum transport of slow charge carriers by Trambly de Laissardière *et al.*,[19] applicable to metallic alloys and compounds in which the electron mean-free path l between the scattering events is small compared to the extension of the conduction-electron wave packet, in which case the electron propagation is non-Boltzmann (nonballistic) and the resistivity exhibits a NTC. The structural and chemical disorders in the Taylor phase due to the fractional and mixed occupancy of the lattice sites imply that the relaxation time τ between the scattering events is short, so that $l=v\tau$ (where v is the electron velocity) is small and the short mean-free-path limit is met, hence justifying the use of the quantum transport theory. This theory has recently been successfully applied to the Al_4(Cr,Fe) decagonal approximant,[7,8] where the temperature-dependent resistivity exhibited a maximum.

In an anisotropic crystal, the electrical conductivity σ (the inverse resistivity $\sigma=\rho^{-1}$) is generally a symmetric (and diagonalizable) tensor, relating the current density $\vec{j}$ to the electric field $\vec{E}$ via the relation $j_i=\Sigma_j\sigma_{ij}E_j$, where $i,j=x,y,z$ denote three orthogonal directions in a Cartesian coordinate system. The tensorial ellipsoid exhibits the same symmetry axes as the crystallographic structure. For our orthorhombic T-Al_3(Mn,Fe) crystal this implies that the conductivity tensor is diagonal in the basis of the crystallographic directions a, b, and c. The geometry of our samples (their long axes were along the three crystallographic directions) and the direction of the electric field applied along their long axes imply that diagonal elements $\sigma_{xx}=\sigma_a$, $\sigma_{yy}=\sigma_b$, and $\sigma_{zz}=\sigma_c$ were measured in our experiments, so that the entire conductivity tensor was determined. The quantum theory of slow charge carriers applies to any diagonal element of the conductivity tensor (in Ref. 19, σ_{xx} is considered, but x can be any crystallographic direction).

According to the Einstein relation, the conductivity σ depends on the electronic density of states (DOS) $g(\varepsilon)$ and the spectral diffusivity $D(\varepsilon)$ within the thermal interval of a few k_BT around the Fermi level ε_F. In the case of slowly varying metallic DOS around ε_F it is permissible to replace $g(\varepsilon)$ by $g(\varepsilon_F)$. For the diffusion constant of slow charge carriers it was shown[19] that it can be written as $D=v^2\tau+L^2(\tau)/\tau$, where $L^2(\tau)$ is the nonballistic (non-Boltzmann) contribution to the square of spreading of the quantum state at energy ε due to diffusion, averaged on a time scale τ. $L(\tau)$ is bounded by the unit cell length and saturates to a constant value already for short averaging time. The dc conductivity of the system in the crystallographic direction j can be written as[19]

$$\sigma_j=\sigma_{Bj}+\sigma_{NBj}=e^2g(\varepsilon_F)v_j^2\tau_j+e^2g(\varepsilon_F)\frac{L_j^2(\tau_j)}{\tau_j}, \qquad (2)$$

where σ_{Bj} is the Boltzmann contribution and σ_{NBj} is the non-Boltzmann contribution. The scattering rate τ^{-1} will generally be a sum of a temperature-independent rate τ_0^{-1} due to scattering by quenched defects and a temperature-dependent rate τ_p^{-1} due to scattering by phonons and the magnetic scattering by localized paramagnetic spins. The anisotropy of the atomic structure implies that the density of quenched defects and the phonon spectrum will also be anisotropic, so that the scattering rate will generally depend on the crystalline direction, $\tau_j^{-1}=\tau_{0j}^{-1}+\tau_{pj}^{-1}$. In the simplest case, τ_{pj} can be phenomenologically written as a power law of temperature, $\tau_{pj}=\beta_j/T^{\alpha_j}$, at least within a limited temperature interval. Assuming that $L_j^2(\tau_j)$ can be replaced by its limiting value, a constant L_j^2, Eq. (2) yields a minimum in the conductivity σ_j as a function of τ_j or temperature (or equivalently, there is a maximum in the resistivity) at the condition $\tau_j=L_j/v_j$. At temperatures below the resistivity maximum, τ_j is long enough that the system is in the Boltzmann regime ($\sigma_j\approx\sigma_{Bj}$) with ballistic propagation of the electrons and a power-law positive-temperature-coefficient (PTC) metallic resistivity. At high temperatures above the resistivity maximum, τ_j is short enough that the system is in the non-Boltzmann (nonballistic) regime and Eq. (2) yields the conductivity of the form

$$\sigma_j=B_j(1+C_jT^{\alpha_j}) \qquad (3)$$

with $B_j=e^2g(\varepsilon_F)L_j^2/\tau_{0j}$ and $C_j=\tau_{0j}/\beta_j$ that describes an insulator-like NTC resistivity. The fits of the anisotropic resistivity of T-$Al_{72.5}Mn_{21.5}Fe_{6.0}$ using Eq. (3) are shown by solid curves in Fig. 5 and the fit parameters are given in Table I. Successful fits down to the lowest investigated temperature of 2 K demonstrate that the degree of structural and chemical disorder in the T-Al_3(Mn,Fe) phase is large enough that the system is in the non-Boltzmann regime

TABLE I. Fit parameters of the electrical resistivity [solid curves in Fig. 5, as calculated from Eq. (3)]. The units of the coefficients C_j are chosen such that the temperature in the product $C_j T^{\alpha_j}$ is dimensionless.

Crystallographic direction *a*		
B_a ($\mu\Omega$ cm)$^{-1}$	C_a	α_a
1.33×10^{-3}	7.5×10^{-3}	0.74
Crystallographic direction *b*		
B_b ($\mu\Omega$ cm)$^{-1}$	C_b	α_b
1.63×10^{-3}	1.1×10^{-2}	0.63
Crystallographic direction *c*		
B_c ($\mu\Omega$ cm)$^{-1}$	C_c	α_c
1.39×10^{-3}	8.1×10^{-3}	0.71

within the whole investigated temperature range.

C. Thermoelectric power

The thermoelectric power (the Seebeck coefficient S) of the T-$Al_{72.5}Mn_{21.5}Fe_{6.0}$ single crystal was measured between 300 and 2 K by using a standard temperature-gradient technique. The thermopower data, measured along the three crystallographic directions *a*, *b*, and *c*, are displayed in Fig. 6. For all three directions, the thermopower is positive with the RT values around 9 μV/K. Within the experimental precision, there is little or no anisotropy in the thermopower. Unlike the electrical resistivity that does not distinguish between the negative (electrons) and positive (holes) charge carriers [the electric charge in Eq. (2) appears as e^2 and is thus insensitive to the sign of the charge], the charge in the expression for the thermopower appears as $1/e$, hence distinguishing between the electrons and holes. For that reason, the thermopower reflects better the anisotropy of the Fermi surface of a complex metallic alloy that generally contains electronlike and holelike parts. The almost isotropic thermopower of Fig. 6 indicates that the anisotropy of the Fermi surface of T-$Al_{72.5}Mn_{21.5}Fe_{6.0}$ is small. Moreover, the positive sign of the thermopower indicates that the holelike parts are dominant.

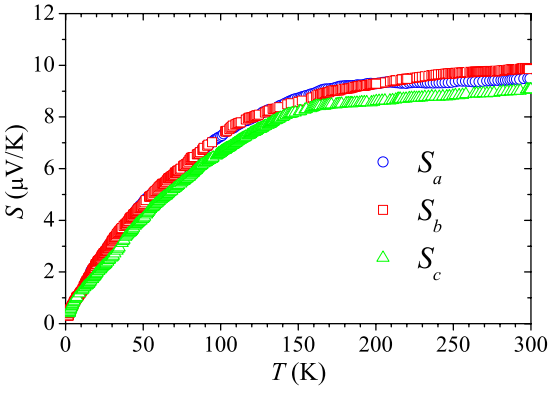

FIG. 6. (Color online) Temperature-dependent anisotropic thermoelectric power (the Seebeck coefficient S) of T-$Al_{72.5}Mn_{21.5}Fe_{6.0}$ along the three orthogonal crystallographic directions *a*, *b*, and *c*.

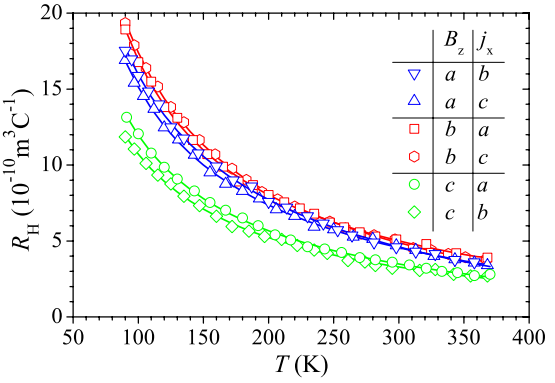

FIG. 7. (Color online) Anisotropic temperature-dependent Hall coefficient $R_H = E_y/j_x B_z$ of T-$Al_{72.5}Mn_{21.5}Fe_{6.0}$ for different combinations of directions of the current j_x and magnetic field B_z (given in the legend).

D. Hall coefficient

Hall coefficient is another physical quantity that distinguishes between the electrons and holes. The Hall-coefficient measurements were performed by the five-point method using standard ac technique in magnetic fields up to 1 T. The current through the samples was in the range 10–50 mA. The measurements were performed in the temperature interval from 90 to 370 K. Using the usual geometry for the Hall effect measurements of a rectangular specimen, where the magnetic field B_z is applied along the z direction, the current density j_x is fed along the x direction and the Hall transverse electric field E_y is generated along the y direction, the Hall coefficient is defined as $R_H = E_y/j_x B_z$. In order to determine the anisotropy of R_H, three sets of experiments were performed with the current j_x along the long axis of each sample (thus along *a*, *b*, and *c*, respectively), whereas the magnetic field B_z was directed along each of the other two orthogonal crystallographic directions, making six experiments altogether. The experimental uncertainty in R_H was $\pm 0.1 \times 10^{-10}$ m^3 C^{-1}.

The anisotropic temperature-dependent Hall coefficient of the T-$Al_{72.5}Mn_{21.5}Fe_{6.0}$ is shown in Fig. 7. The six R_H sets of data form three groups of two approximately identical R_H curves, where the magnetic field in a given crystallographic direction yields, in accordance with the Onsager relations,[20] the same R_H for the current along the other two crystallographic directions in the perpendicular plane. Thus, approximately identical Hall coefficients are obtained for the pair combinations $E_b/j_c B_a = E_c/j_b B_a = R_H^a$ (where the additional superscript on the Hall coefficient denotes the direction of the magnetic field), $E_a/j_c B_b = E_c/j_a B_b = R_H^b$ and $E_b/j_a B_c = E_a/j_b B_c = R_H^c$. All Hall coefficients strongly increase upon cooling and their temperature-dependence resembles that of the Curie-type magnetic susceptibility χ within the paramagnetic phase, shown in Fig. 4(a). This indicates that the anomalous (magnetic) contribution to the Hall coefficient is dominant, to be discussed in the following.

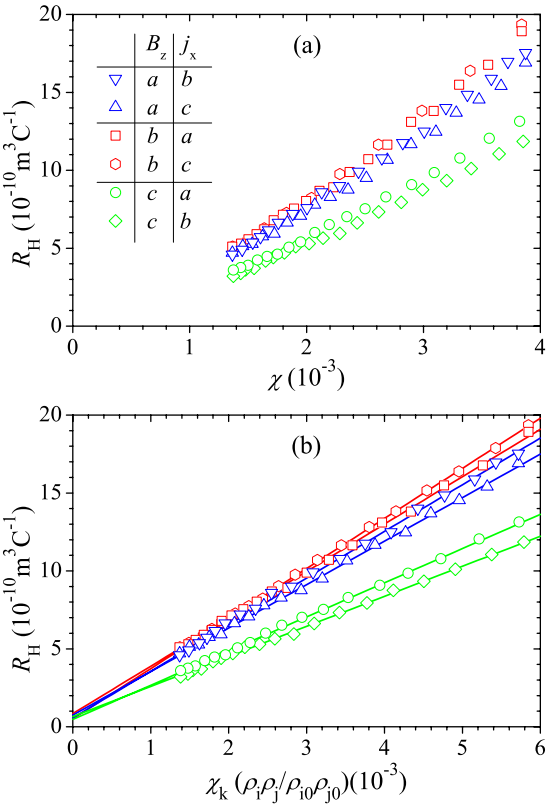

FIG. 8. (Color online) (a) The anisotropic Hall coefficient R_H^k of T-$Al_{72.5}Mn_{21.5}Fe_{6.0}$ as a function of the paramagnetic susceptibility χ_k from Fig. 4(a) for different combinations of directions of the current j_x and magnetic field B_z (given in the legend). (b) The Hall coefficient as a function of $\chi_k(\rho_i\rho_j/\rho_{i0}\rho_{j0})$, where i, j denote the two orthogonal crystallographic directions perpendicular to the magnetic field direction k. $\rho_{i0}\rho_{j0}$ are arbitrary chosen RT (T=295 K) values of the electrical resistivity. The legend in the panel (b) is the same as in (a).

In paramagnetic solids with the small-enough susceptibility that the demagnetization fields can be neglected (which is the case for our sample), the anisotropic Hall coefficient for the magnetic field along the k direction can be written as[21]

$$R_H^k = R_0^k + \chi_k R_S^k, \tag{4}$$

where R_0^k is the normal Hall coefficient due to the Lorentz force and R_S^k is the anomalous Hall coefficient, originating from the magnetization. Due to the second term in Eq. (4), R_H^k follows the strong Curie-Weiss temperature dependence of χ_k. In order to separate the normal and anomalous Hall coefficients, R_H^k is plotted versus the susceptibility χ_k. Assuming temperature-independent R_0^k and R_S^k coefficients, R_0^k is derived from the intercept and R_S^k from the slope of the $R_H^k(\chi_k)$ line. Using the paramagnetic susceptibility from Fig. 4(a), the $R_H^k(\chi_k)$ plots for all combinations of the current and field directions are shown in Fig. 8(a). Although the R_H^k curves seem fairly linear in χ_k, a closer inspection reveals clear deviation from linearity, demonstrating that the assumption of temperature-independent R_0^k and R_S^k is not justified. R_0^k should show strong temperature dependence only in the case of unequal and strongly temperature-dependent relaxation times of the electrons and holes, but this should also yield a strong temperature dependence of the electrical resistivity. For our T-$Al_{72.5}Mn_{21.5}Fe_{6.0}$, the electrical resistivity increase between RT and 90 K (within the temperature range of the Hall-coefficient experiment) is by about 20%, whereas the anisotropic Hall coefficients increase in the same temperature range for much larger factors of about 3.5. A significant contribution of R_0^k to the strong temperature dependence of R_H^k is thus unlikely and can be neglected with respect to that of R_S^k, so that our further analysis is performed by assuming a temperature-independent R_0^k and a temperature-dependent R_S^k.

TABLE II. Normal Hall coefficient R_0 and the RT value of the anomalous Hall coefficient $R_{S,295\ K}$ of the single-crystalline T-$Al_{72.5}Mn_{21.5}Fe_{6.0}$ for various directions of the electrical current and magnetic field. The values were deduced from the R_H^k versus $\chi_k(\rho_i\rho_j/\rho_{i0}\rho_{j0})$ plots, where k denotes the direction of the magnetic field and i, j denote the two orthogonal crystallographic directions perpendicular to the magnetic field. $\rho_{i0}\rho_{j0}$ are arbitrary chosen RT (T=295 K) values of the electrical resistivity.

Field direction (B_z)	Current direction (j_x)	R_0 (10^{-10} m^3 C^{-1})	$R_{S,295\ K}$ (10^{-7} m^3 C^{-1})
a	*b*	0.6	3.0
	c	0.8	2.8
b	*a*	0.8	3.0
	c	0.6	3.2
c	*a*	0.5	2.2
	b	0.7	1.9

It is generally accepted[22] that in metallic systems with a high resistivity, the anomalous Hall effect is dominated by a side-jump mechanism, i.e., by a lateral displacement that the electrons undergo during scattering in the presence of spin-orbit interaction.[23] In that case, the anomalous Hall coefficient should be proportional to the square of the resistivity, $R_S \propto \rho^2$, so that a temperature-dependent $\rho(T)$ results in a temperature-dependent $R_S(T)$.[24] In an anisotropic crystal, ρ^2 is replaced by the product $\rho_i\rho_j$, where i, j denote the two orthogonal crystallographic directions perpendicular to the magnetic field direction k. By suitably normalizing to the RT (T=295 K) values, denoted here as $\rho_{i0}\rho_{j0}$, Eq. (4) can be rewritten as

$$R_H^k = R_0^k + R_{S,295\ K}^k \cdot \chi_k(\rho_i\rho_j/\rho_{i0}\rho_{j0}), \tag{5}$$

where $R_{S,295\ K}^k$ is the value of the anomalous Hall coefficient R_S^k at 295 K. In Fig. 8(b) we plotted R_H^k as a function of $\chi_k(\rho_i\rho_j/\rho_{i0}\rho_{j0})$. In this plot, the anisotropic R_H^k curves show well-defined linearity, enabling us to extract the R_0^k and $R_{S,295\ K}^k$ parameters. These parameter values, for all combinations of the current and field directions, are listed in Table II. The differences of the two R_0^k or $R_{S,295\ K}^k$ values for a particular field direction are small enough to be ascribed to the experimental error. The R_0^k values are positive for all three crystallographic directions and in the range $[0.5,0.8] \times 10^{-10}$ m^3 C^{-1}. The positive sign of the normal Hall coefficient indicates that holes are the dominant charge carriers,

in agreement with the positive hole-type thermoelectric power from Fig. 6. The above R_0^k magnitude of the order 10^{-10} m^3 C^{-1} yields the effective charge-carrier density of the order 10^{23} cm^{-3}, a typical metallic value. Within the experimental error, no anisotropy of the normal Hall coefficient R_0^k can be claimed. The $R_{S,295\ \mathrm{K}}^k$ values are, on the other hand, of the order 10^{-7} m^3 C^{-1} and show small, but distinct anisotropy. The highest value $R_{S,295\ \mathrm{K}}^b=(3.1\pm0.1)\times10^{-7}$ m^3 C^{-1} is obtained for the field along the b direction, where the in-plane product $\rho_a\rho_c$ is the largest according to the anisotropic resistivities shown in Fig. 5. This supports the consideration that the anisotropy of the resistivity is the dominant cause of the anisotropy of the anomalous Hall coefficient R_S^k. We emphasize that the $R_{S,295\ \mathrm{K}}^k$ values are rather large, which is certainly due to the high resistivity of the T-$Al_{72.5}Mn_{21.5}Fe_{6.0}$ compound that amounts at RT (depending on the crystallographic direction) between 440 and 500 $\mu\Omega$ cm. The obtained $R_{S,295\ \mathrm{K}}^k$ values are close to those determined for the T-$Al_{80}Mn_{20}$, T-$Al_{78}Mn_{22}$, and T-$Al_{73}Mn_{27}$ phases, amounting (3.2, 4.8, and 3.5) $\times10^{-7}$ m^3 C^{-1}, respectively.[25,17] For comparison, amorphous ferromagnetic alloys with lower resistivities around 150 $\mu\Omega$ cm show smaller R_S of the order 10^{-8} m^3 C^{-1},[23] whereas for the high-resistivity icosahedral quasicrystal $Al_{70.4}Pd_{20.8}Mn_{8.8}$ with $\rho_{RT}\approx1000$ $\mu\Omega$ cm, a higher value $R_S=1.8\times10^{-5}$ m^3 C^{-1} was reported,[26] showing clearly the influence of the resistivity magnitude on R_S.

A basic discrepancy between the Hall-coefficient measurements on the single-crystalline T-$Al_{72.5}Mn_{21.5}Fe_{6.0}$ and the polygrain Taylor-phase samples studied in Ref. 15 is the sign of the normal Hall coefficient, which is positive holelike for the single crystal and negative electronlike (or the coefficient value is close to zero for some chemical compositions) for the polygrain T-Al_3Mn, T-$Al_{73}Mn_{27-x}Fe_x$ ($x=2,4$) and d-$Al_{73}Mn_{21}Fe_6$. Since the positive holelike normal Hall coefficient of the single-crystalline T-$Al_{72.5}Mn_{21.5}Fe_{6.0}$ is in agreement with the positive holelike thermopower of this compound, the results of the single crystal should be trusted.

To summarize, the Hall coefficient of the single-crystalline T-$Al_{72.5}Mn_{21.5}Fe_{6.0}$ is dominated by the magnetic anomalous contribution and shows strong temperature dependence. For all three directions of the magnetic field B_z, the Hall coefficient $R_H(T)$ is a linear function of $\chi_z\rho_x\rho_y$. This enables the separation of the normal and anomalous Hall coefficients R_0 and R_S. The values of the normal Hall coefficient R_0 are typical metallic of about $(0.7\pm0.1)\times10^{-10}$ m^3 C^{-1} and do not exhibit anisotropy within the experimental error. The positive sign of R_0 indicates that holes are the majority charge carriers, in agreement with the hole-type positive thermopower of this compound. The anomalous Hall coefficient R_S is very large due to the high resistivity of the compound, with the RT value of the order 10^{-7} m^3 C^{-1}. It exhibits a weak anisotropy that can be attributed to the weak anisotropy of the electrical resistivity.

E. Thermal conductivity

Thermal conductivity κ of the T-$Al_{72.5}Mn_{21.5}Fe_{6.0}$ single crystal was measured along the a, b, and c directions using an absolute steady-state heat-flow method. The thermal flux through the samples was generated by a 1 kΩ RuO_2 chip resistor, glued to one end of the sample, while the other end was attached to a copper heat sink. The temperature gradient across the sample was monitored by a chromel-constantan differential thermocouple. The anisotropic total thermal conductivities κ_a, κ_b, and κ_c along the three crystallographic directions, normalized to their 300 K values, are displayed in Fig. 9. The normalization was employed to show that the temperature-dependences of κ_a, κ_b, and κ_c are practically the same within the experimental error. The absolute values at $T=300$ K amount $\kappa_a^{300\ \mathrm{K}}=3.7$ W/mK, $\kappa_b^{300\ \mathrm{K}}=3.2$ W/mK, and $\kappa_c^{300\ \mathrm{K}}=3.2$ W/mK, so that the anisotropy of the thermal conductivity is practically negligible.

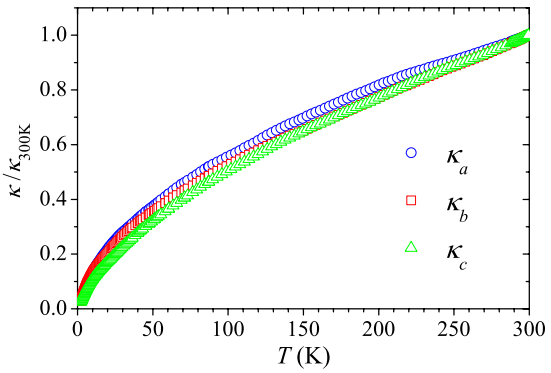

FIG. 9. (Color online) The anisotropic thermal conductivities κ_a, κ_b, and κ_c of T-$Al_{72.5}Mn_{21.5}Fe_{6.0}$ along the three crystallographic directions, normalized to their 300 K values.

The electronic contribution κ_{el} to the total thermal conductivity can be estimated from the Wiedemann-Franz (WF) law, $\kappa_{el}=\pi^2k_B^2T\sigma(T)/3e^2$, and the measured electrical conductivity data $\sigma(T)$. Here it is important to recall the validity of the WF law,[27] which is valid under the condition of dominant elastic scattering of the electrons, usually realized at high temperatures $T>\theta_D$, where θ_D is the Debye temperature (e.g., for typical metals, the WF law is valid already at RT). At low temperatures, the WF law is valid for solids where only the residual electrical resistivity (due to elastic scattering by quenched defects) is observed. The strongly temperature-dependent NTC resistivity of the T-$Al_{72.5}Mn_{21.5}Fe_{6.0}$ single crystal from Fig. 5 suggests that the WF law in not applicable at temperatures below RT, so that we use it only to estimate the RT κ_{el} values. Taking the 300 K ρ values from Fig. 5, we obtain the electronic thermal conductivities at $T=300$ K as $\kappa_{el}^a=1.5$ W/mK, $\kappa_{el}^b=1.6$ W/mK, and $\kappa_{el}^c=1.5$ W/mK. This gives the RT ratios of the electronic to the total thermal conductivity as $(\kappa_{el}^a/\kappa_a)_{300\ \mathrm{K}}=0.41$, $(\kappa_{el}^b/\kappa_b)_{300\ \mathrm{K}}=0.50$, and $(\kappa_{el}^c/\kappa_c)_{300\ \mathrm{K}}=0.47$, so that at RT, the electrons and holes carry about half of the heat, the other half being transported by the lattice.

IV. SUMMARY AND CONCLUSIONS

We have investigated the magnetic susceptibility, the electrical resistivity, the thermoelectric power, the Hall coefficient and the thermal conductivity of the Taylor-phase

T-$Al_{72.5}Mn_{21.5}Fe_{6.0}$ complex intermetallic compound that is an orthorhombic approximant to the *d*-Al-Mn-Pd decagonal quasicrystal with six atomic layers within one periodic unit of 1.24 nm and 156 atoms in the giant unit cell. The main objective was to determine the crystallographic-direction-dependent anisotropy of the investigated physical parameters when measured within the (a,c) atomic planes, corresponding to the quasiperiodic planes in the related *d*-QCs, and along the stacking *b* direction perpendicular to the planes, corresponding to the periodic direction in *d*-QCs.

The T-$Al_{72.5}Mn_{21.5}Fe_{6.0}$ shows spin-glass behavior below the spin-freezing temperature $T_f \approx 29$ K. The orientation-dependent magnetic susceptibilities do not show anisotropy for the magnetic field applied along the two in-plane directions *a* and *c*, whereas there exists a moderate anisotropy between the in-plane and the stacking *b* directions, where the susceptibility along *b* is somewhat higher. The temperature-dependent susceptibility difference $\chi_{\mathrm{fc}}-\chi_{\mathrm{zfc}}$ below T_f does not show anisotropy and there is also no anisotropy in the spin-freezing temperature, the $M(H)$ hysteresis curves and the memory effect for the three crystallographic directions.

The anisotropic electrical resistivities are rather large (the RT values in the range 440–500 $\mu\Omega$ cm) and show a NTC along all three crystallographic directions. The resistivity is the lowest along the stacking *b* direction perpendicular to the atomic planes, whereas the two in-plane resistivities ρ_a and ρ_c are at RT about 10% higher and show almost no anisotropy. It is remarkable that this kind of anisotropy, where the resistivity is the lowest along the stacking direction, appears to be a general feature of the decagonal-approximant phases with the stacked-layer structure. The NTC resistivity was theoretically reproduced by the quantum transport theory of slow charge carriers, applicable to metallic alloys and compounds in which the electron mean-free path *l* between the scattering events is small compared to the extension of the conduction-electron wave packet, in which case the electron propagation is non-Boltzmann (nonballistic) and the resistivity exhibits a NTC. The short mean-free path in the Taylor-phase crystals is a consequence of structural and chemical disorder on the lattice, as most of the lattice sites show either fractional occupation or mixed TM/Al occupancy.

The thermopower is positive for all three crystallographic directions and no anisotropy can be claimed within the experimental precision. The almost isotropic thermopower indicates that the anisotropy of the Fermi surface of the T-$Al_{72.5}Mn_{21.5}Fe_{6.0}$ is small, whereas its positive sign indicates that the holelike parts of the Fermi surface are dominant.

The same conclusion on the holes being the dominant charge carriers in the T-$Al_{72.5}Mn_{21.5}Fe_{6.0}$ is inferred from the Hall-coefficient measurements. The anisotropic Hall coefficient is a sum of the normal Hall coefficient due to the Lorentz force and the anomalous term, originating from the magnetization. The anomalous term introduces strong temperature dependence into the Hall coefficient, originating from both the temperature-dependent magnetic susceptibility and the temperature-dependent electrical resistivity. The anomalous Hall coefficient exhibits a weak anisotropy that can be attributed to the weak anisotropy of the electrical resistivity. The normal Hall coefficient is temperature independent and positive, confirming that the holes are the dominant charge carriers. It shows no anisotropy for different combinations of the magnetic field and electric current directions.

The anisotropy of the thermal conductivity of T-$Al_{72.5}Mn_{21.5}Fe_{6.0}$ along the three crystallographic directions is practically negligible. An estimation of the electronic contribution to the total thermal conductivity by using the Wiedemann-Franz law suggests that at RT, the electrons and holes carry about half of the heat, the other half being transported by the lattice.

The anisotropy of the investigated magnetic, electrical and thermal transport properties of the Taylor-phase T-$Al_{72.5}Mn_{21.5}Fe_{6.0}$ decagonal approximant with six atomic layers within one periodic unit along the stacking direction is small or in some cases negligible within the experimental precision (the thermopower and the thermal conductivity). This result should be contrasted with the anisotropic properties of the decagonal approximants from the $Al_{13}TM_4$ family, where the Y-Al-Ni-Co two-layer compound[3,4] and the o-$Al_{13}Co_4$ (Ref. 5), $Al_{13}Fe_4$, and $Al_{13}(Fe,Ni)_4$ (Ref. 6) four-layer compounds all show significant anisotropies along the three orthogonal crystallographic directions. However, the $Al_4(Cr,Fe)$ (Refs. 7 and 8) six-layer decagonal approximant from the Al_4TM family shows anisotropy of a similar magnitude to those observed for the above two- and four-layer $Al_{13}TM_4$ phases. The presumable rule that the increasing number of atomic layers within one periodic unit decreases the anisotropy of the tensorial physical properties of a decagonal-approximant phase with a stacked-layer structure is thus not generally valid, but the degree of anisotropy rather depends on the structural and chemical details of a particular phase. Our investigation presents experimental evidence that the Taylor-phase six-layer decagonal approximant shows the smallest anisotropy of all the so-far investigated stacked-layer decagonal-approximant phases. The Taylor phase can thus be considered as a "close-to-isotropic" compound. The decisive role of the structural and chemical details of a particular phase for its physical properties is also supported by the fact that the properties of the Taylor phase T-$Al_{72.5}Mn_{21.5}Fe_{6.0}$ are in many respects very different from those of the $Al_{13}TM_4$ and Al_4TM families. Although all these phases contain a significant fraction of a magnetic transition metal (Mn, Fe, Co), the Taylor phase is the only one to show strong Curie-type paramagnetism and a spin glass transition at low temperatures. The NTC resistivity of the Taylor phase is also different from the PTC resistivity of the $Al_{13}TM_4$ phases, whereas the anisotropic resistivities of the $Al_4(Cr,Fe)$ exhibit a maximum with the transition from NTC to PTC upon cooling. The Taylor phase is also the only one to show the dominant anomalous contribution to the Hall coefficient. Therefore, no common footing of the anisotropic

physical properties of the stacked-layer decagonal-approximant phases from different structural families can be inferred.

ACKNOWLEDGMENTS

This work was done within the activities of the 6th Framework EU Network of Excellence "Complex Metallic Alloys" (Contract No. NMP3-CT-2005-500140). Croatian authors (J.I., P.P., I.B. and A.S.) acknowledge support of the Ministry of Science, Education and Sports of the Republic of Croatia through the Research Projects No. 035-0352826-2848 and No. 119-1191458-0512. M.H. and M.F. acknowledge the grant by the Deutsche Forschungsgemeinschaft (PAK 36).

*On leave from the Institute of Molecular Physics, Polish Academy of Sciences, Smoluchowskiego 17, 60-179 Poznań, Poland.

[1] M. Krajčí and J. Hafner, Phys. Rev. B **58**, 5378 (1998).
[2] G. Trambly de Laissardière and T. Fujiwara, Phys. Rev. B **50**, 9843 (1994).
[3] A. Smontara, I. Smiljanić, J. Ivkov, D. Stanić, O. S. Barišić, Z. Jagličić, P. Gille, M. Komelj, P. Jeglič, M. Bobnar, and J. Dolinšek, Phys. Rev. B **78**, 104204 (2008).
[4] M. Komelj, J. Ivkov, A. Smontara, P. Gille, P. Jeglič, and J. Dolinšek, Solid State Commun. **149**, 515 (2009).
[5] J. Dolinšek, M. Komelj, P. Jeglič, S. Vrtnik, D. Stanić, P. Popčević, J. Ivkov, A. Smontara, Z. Jagličić, P. Gille, and Yu. Grin, Phys. Rev. B **79**, 184201 (2009).
[6] P. Popčević, A. Smontara, J. Ivkov, M. Wencka, M. Komelj, P. Jeglič, S. Vrtnik, M. Bobnar, Z. Jagličić, B. Bauer, P. Gille, H. Borrmann, U. Burkhardt, Yu. Grin, and J. Dolinšek, preceding paper, Phys. Rev. B **81**, 184203 (2010).
[7] J. Dolinšek, P. Jeglič, M. Komelj, S. Vrtnik, A. Smontara, I. Smiljanić, A. Bilušić, J. Ivkov, D. Stanić, E. S. Zijlstra, B. Bauer, and P. Gille, Phys. Rev. B **76**, 174207 (2007).
[8] J. Dolinšek, S. Vrtnik, A. Smontara, M. Jagodič, Z. Jagličić, B. Bauer, and P. Gille, Philos. Mag. **88**, 2145 (2008).
[9] D. W. Deng, Z. M. Mo, and K. H. Kuo, J. Phys.: Condens. Matter **16**, 2283 (2004).
[10] K. Hiraga, M. Kaneko, Y. Matsuo, and S. Hashimoto, Philos. Mag. B **67**, 193 (1993).
[11] H. Klein, M. Boudard, M. Audier, M. de Boissieu, H. Vincent, L. Beraha, and M. Duneau, Philos. Mag. Lett. **75**, 197 (1997).
[12] S. Balanetskyy, G. Meisterernst, M. Heggen, and M. Feuerbacher, Intermetallics **16**, 71 (2008).
[13] M. A. Taylor, Acta Crystallogr. **14**, 84 (1961).
[14] P. Priputen, M. Kusý, M. Kriška, R. Lipka, E. Illeková, P. Švec, J. Buršík, M. Svoboda, J. Dolinšek, and J. Janovec, Intermetallics **17**, 1047 (2009).
[15] J. Dolinšek, J. Slanovec, Z. Jagličić, M. Heggen, S. Balanetskyy, M. Feuerbacher, and K. Urban, Phys. Rev. B **77**, 064430 (2008).
[16] J. Dolinšek, M. Feuerbacher, M. Jagodič, Z. Jagličić, M. Heggen, and K. Urban, J. Appl. Phys. **106**, 043917 (2009).
[17] D. Stanić, J. Ivkov, A. Smontara, Z. Jagličić, J. Dolinšek, M. Heggen, and M. Feuerbacher, Z. Kristallogr. **224**, 49 (2009).
[18] P. W. Selwood, *Magnetochemistry* (Interscience Publishers, New York, 1956), p. 78.
[19] G. Trambly de Laissardière, J.-P. Julien, and D. Mayou, Phys. Rev. Lett. **97**, 026601 (2006).
[20] A. C. Smith, J. F. Janak, and R. B. Adler, *Electronic Conduction in Solids* (McGraw-Hill, New York, 1967), p. 226.
[21] C. M. Hurd, *The Hall Effect in Metals and Alloys* (Plenum, New York, 1972).
[22] T. R. McGuire, R. J. Gambino, and R. C. O'Handley, in *The Hall Effect and its Applications*, edited by C. L. Chien and C. R. Wetsgate (Plenum, New York, 1980), p. 137.
[23] L. Berger, Phys. Rev. B **2**, 4559 (1970).
[24] N. A. Sinitsyn, J. Phys.: Condens. Matter **20**, 023201 (2008).
[25] A. Gozlan, C. Berger, G. Fourcaudot, R. Omari, J. C. Lasjaunias, and J. J. Préjean, Phys. Rev. B **44**, 575 (1991).
[26] A. Poddar, S. Das, D. Plachke, and H. D. Carstanjen, J. Magn. Magn. Mater. **300**, 263 (2006).
[27] U. Mizutani, *Introduction to the Electron Theory of Metals* (Cambridge University Press, Cambridge, England, 2001), p. 299.